Available online at www.sciencedirect.com

ScienceDirect

Ceramics International 40 (2014) 1051–1058

CERAMICS INTERNATIONAL

www.elsevier.com/locate/ceramint

Grain growth in $BaTiO_3$ ceramics assisted by an intergranular glass film

Chih-Hung Nien*, Cheng-Yan Hsieh, Jiang-Yu Hong, Hong-Yang Lu

Center for NanoScience and Department of Materials Science, National Sun Yat-Sen University, Kaohsiung 80424, Taiwan

Received 18 April 2013; received in revised form 27 June 2013; accepted 27 June 2013
Available online 3 July 2013

Abstract

This research demonstrates that $BaTiO_3$ ceramics exhibit increased grain boundary mobility (M_b) triggered by an inter-granular glass film (IGF) as previously demonstrated in polycrystalline Al_2O_3 ceramics conversion to single-crystal sapphire upon annealing at high temperatures. These results suggest that secondary abnormal grain growth (SAGG) during sintering of $BaTiO_3$ ceramics at 1365 °C, a temperature above the eutectic points in the $BaTiO_3$–SiO_2 and $BaTiO_3$–TiO_2 systems, is another example of faster M_b caused by IGF. Higher M_b magnified through an interface glass film of several nanometers thickness facilitates a faster grain growth rate that produces exceedingly large grains of ~2.4 mm in size. The growth mechanism involving twin-plane re-entrant (TPRE) corners may not be the only route responsible for SAGG in $BaTiO_3$, particularly when sintered at above eutectic temperatures. How this abnormal grain growth occurs through mechanisms involving liquid-phase-enhanced M_b and the {111} twins as a chemically induced growth fault is discussed.

Keywords: A. Grain growth; B. Electron microscopy; D. $BaTiO_3$

1. Introduction

Extraordinarily large grains of several centimeters in size were obtained [1–3] when nearly stoichiometric $BaTiO_3$ powder (i.e., slightly TiO_2-excess of Ba/Ti=0.999) infiltrated with a slurry containing 1 mol% of SiO_2 and TiO_2 was sintered at 1350 °C for 8 h in air [1]. A similar discovery was made by Yamamoto et al. [4] several years earlier who also used slightly TiO_2-excess powder in sintering. A route preparing $BaTiO_3$ single crystals through solid-state crystal growth from polycrystalline $BaTiO_3$ was suggested. Although the growth mechanism for $BaTiO_3$ was not addressed specifically [4], it was a similar process resembling the conversion of polycrystalline alumina into single-crystal sapphire [5–7] where a minute amount of liquid phase [7] may have played a decisive role. In order to differentiate from the conventional abnormal grain growth (AGG), this exceptional behavior observed [1–4] in $BaTiO_3$ was termed the secondary abnormal grain growth (SAGG). In contrast, conventional AGG leading to the microstructure of a bimodal grain size distribution [8] in $BaTiO_3$ where large grains are usually lamellar in shape is referred to as the primary abnormal grain growth (PAGG).

Two key factors that catalyzed SAGG in $BaTiO_3$ were proposed [1–3]: (1) the presence of the {111} double-twin grains, and (2) infiltration with SiO_2 prior to sintering. However, they are mutually related because it was also suggested [1,2] that adding SiO_2 promotes the formation of the {111} double-twin grains. These twin grains then provide the twin-plane re-entrant edges (TPRE) or corners that facilitate perpetuated growth [9–11] of $BaTiO_3$ grains to enormous sizes [1–3]. The mechanism was often called TPRE [1–3]. The argument necessitates that TPRE edges, which are the sites enabling two-dimensional (2D) nucleation, are maintained throughout by heat treatment. The 2D nucleation on TPRE edges is kinetically favorable because it requires considerably less activation enthalpy (ΔH_T, where the subscript T represents TPRE) than that on an atomically flat surface (ΔH_F, the subscript F for flat grain surface). TPRE therefore unleashes a burst out of the nuclei and a growth rate surge leading to unusually large grains.

Munoz-Saldana et al. [12] reproduced SAGG in SiO_2-infiltrated $BaTiO_3$ which was heat-treated at 1260 °C/10 h followed by rising to 1320 °C/5 min, but second phase

*Corresponding author. Tel.: +886 7 5252000x4076; fax: +886 7 5254099.
E-mail address: d983100009@student.nsysu.edu.tw (C.-H. Nien).

0272-8842/$ - see front matter © 2013 Elsevier Ltd and Techna Group S.r.l. All rights reserved.
http://dx.doi.org/10.1016/j.ceramint.2013.06.103

$BaTiSiO_5$ derived from the $BaTiO_3$–SiO_2 liquid eutectic formed at 1260 °C was detected. Double-twin grains although seen in the SiO_2-penetrated region did not exhibit nucleation-favorable [9–11] TPRE corners.

We report on grain growth in $BaTiO_3$ ceramics sintered at 1215 °C, 1265 °C, and 1365 °C in air using both BaO-excess and TiO_2-excess powders. The latter two temperatures are higher than the eutectic points in the $BaTiO_3$–SiO_2 (at 1260 °C [12,13]) and $BaTiO_3$–TiO_2 (at 1332 °C [14]) systems. Experimental results suggest that SAGG is promoted by greater boundary mobility enhanced by a thin liquid film at the interface of growing grains in initially TiO_2-excess $BaTiO_3$. The likelihood that this grain growth mechanism is induced chemically by the {111} growth twins whose boundary is a planar fault is also discussed.

2. Experimental procedure

Commercial $BaTiO_3$ powders (Ticon™ HPB®, Ferro Electronic Material Systems, Penn Yan, NY, USA) prepared via an advanced oxalate route according to the manufacturer, of TiO_2-excess (of Ba/Ti = 0.9889, Lot no. 738, D_{50} = 300 nm) and BaO-excess (of Ba/Ti = 1.0007, Lot no. EXP4763, D_{50} = 256 nm) compositions were used in this study. The major impurities are SiO_2, SrO, MgO, CaO, Fe_2O_3, Na_2O, and K_2O. SiO_2 is most relevant to the present study, which amounts to ~121 ppm (wt.) and ~60 ppm (wt.) in the TiO_2-excess and BaO-excess powder, respectively.

The powders were ball-milled using Y_2O_3-stabilized ZrO_2 balls with alcohol in a polyurethane jar to break up agglomerates before passing through a 125 μm sieve to remove the remaining large ones. A suitable quantity of powders was die-pressed at 100 MPa into disks of 10 mm diameter and ~2 mm thickness using a WC-inserted steel die and punch to make single-layer samples. Double-layer samples consist of BaO-excess single-layer disc on the top with TiO_2-excess single-layer disc beneath it. They were prepared using single-layer discs pre-pressed at 5 MPa before stacking one on top of the other and pressing again at 100 MPa. Samples were packed with either TiO_2-excess or BaO-excess powder, and made to sit in a high-purity Al_2O_3 crucible for sintering at desired temperatures in air using 5 °C/min heating rate before being furnace-cooled to room temperature.

Sintered samples were polished successively using diamond-lapping films, and completed with DuPont™ Syton™ to obtain ~30 nm surface roughness. Polished sections were chemical-etched in a 70% HCl solution added with a few drops of HF to delineate the grain boundaries and ferroelectric domains. Sintered microstructure was examined using reflected light optical microscopy (OM, Nikon, AVK-C2, Tokyo, Japan), scanning electron microscopy (SEM, JEOL™ SEM-6330, Tokyo, Japan) operating at 20 kV, and transmission electron microscopy (TEM, JEOL™ AEM-3010) operating at 300 kV. Both SEM and TEM are equipped with energy-dispersive spectroscopy (EDS, Link Systems, Oxford Instruments, Oxford, UK) for micro-chemical analysis. The average grain size was determined using Optimas® (v6.1, Optimas Co., 1987). A focused ion beam (FIB) instrument (SMI-3050, Seiko, Tokyo, Japan) was used for preparing thin foils because specific locations in samples were required for close examination under TEM.

3. Results

3.1. TiO_2-excess samples sintered at 1215 °C and 1265 °C

Fig. 1(a) shows the SEM secondary electron image (SEI) that reveals [8] how PAGG occurs during TiO_2-excess powder sintering at 1215 °C. Small grains coarsened to particle chains [15] through neck formation are dispersed in a matrix of lamellar {111} twin grains grown from ~10 μm to large sizes of ~15–20 μm by Ostwald ripening when sintering was extended from 20 h to 55 h, 100 h (Fig. 1(a)), and to 300 h [8]. It represents how the microstructure of TiO_2-excess powder sintered at < 1260 °C, the lowest eutectic temperature of 1260 °C [12,13] in the $BaTiO_3$–SiO_2 system was developed, knowing that SiO_2 is an inevitable trace impurity in the initial powder. After annealing for 100 h, lamellar grains coarsened at the expense of small grains and evolved into a skeletal microstructure [8] resembling a house of cards. An intergranular (or interface) glass film (IGF) of ~1.2 nm, which is liquid at the sintering temperature, determining using Digital Micrograph™ (v3.7.4, 1996, Gatan™, Pleasanton, CA, USA),

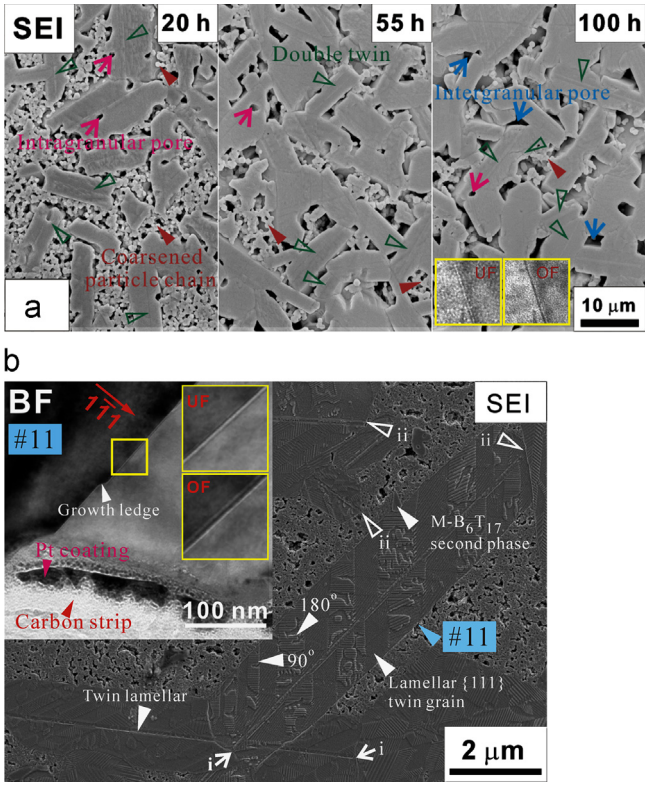

Fig. 1. Sintered microstructure of TiO_2-excess powder: (a) PAGG from 1215 °C/10 h, 55 h, and 100 h (courtesy of Dr. Ming-Hong Lin), and an IGF ~1.2 nm was detected and shown in the inset, (b) PAGG from 1265 °C/20 h (SEM-SEI) where an IGF of ~0.9 nm exists between lamellar grains and the matrix shown in the inset (UF: under focus, OF: over focus, TEM-BF image).

was detected in foil #1, as shown in the inset of SEI for the 100 h samples. Microstructure features of AGG are represented by some residual pores entrapped in the grain interior, producing the distinct grain sizes (Fig. 1(a)). Although double-twins in a considerable quantity (indicated in Fig. 2 (a)) are identified, no SAGG occurs. Even after prolonged sintering for 300 h [8], skeletal microstructure of double-twins and residual pores persisted.

Sintering at 1265 °C/20 h results in a bimodal grain size distribution (Fig. 1(b)) representing PAGG. This is typical of TiO_2-excess powder sintered at temperatures slightly higher than the lowest eutectic point of ~1260 °C [12,13]. Suggestion is that the liquid eutectic involves in developing the microstructure feature. It contains mostly the characteristic {111} double-twin grains grown to the lamellar shape of high-aspect ratio that are scattered in a low sintered density matrix. These twin grains very scarcely contain residual pores. Only occasionally are the TPRE edges (indicated as (i) in Fig. 1(b)) from double-twinned grains thought to sustain perpetual growth [9–11] observed. Other twin lamellae have grown to ridges [9–11], or impinged mutually where the TPRE corners [1–3] were lost (indicated by (ii)).

The 90 ° and 180 ° ferroelectric domains (as indicated) are characterized by herring-bone and water-mark patterns, respectively; observed in the lamellar grains are the representative features of tetragonal-$BaTiO_3$ ceramic [16]. Second phase monoclinic-$Ba_6Ti_{17}O_{40}$ can easily be identified by its dark contrast under SEM-SEI, which is formed when excess TiO_2 reacts with $BaTiO_3$ in solid-state [14]. Residual pores are found predominantly in areas among twin lamellae (Fig. 1(b)) where the microstructure is represented by neck formation and grain coarsening into particle chains [15].

The bimodal microstructure shown in Fig. 1(a) and (b) is often addressed in the literature as PAGG; the densification of both samples is enhanced by eutectic liquids formed at ≤1265 °C. An IGF of ~0.9 nm thickness is determined adopting the Fresnel under-focus (UF) and over-focus (OF) imaging technique [17], as shown in the inset of Fig. 1(b).

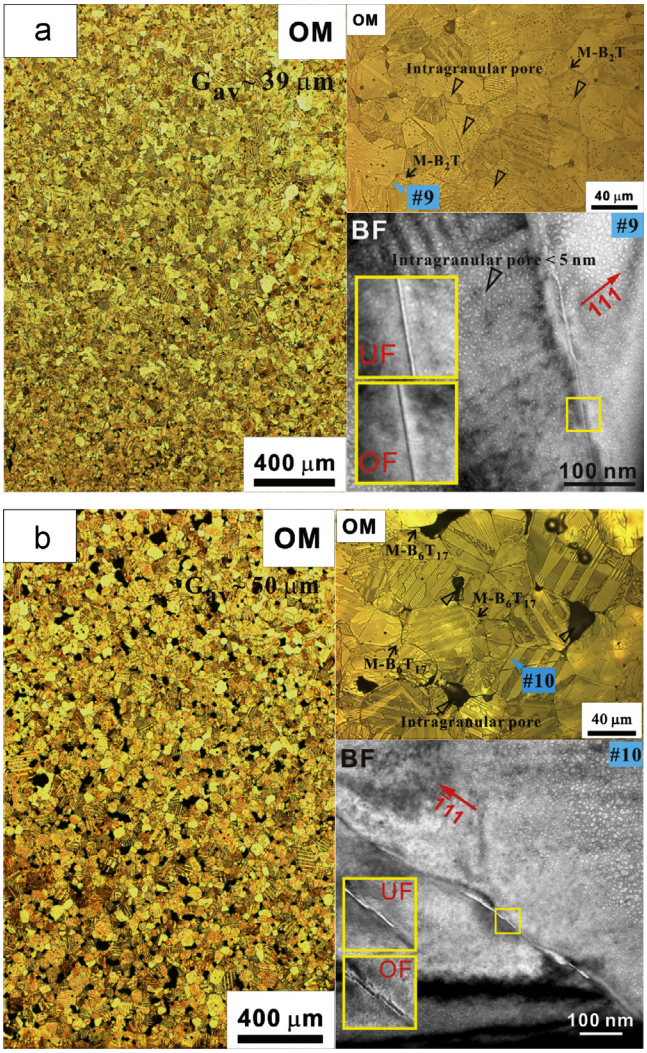

Fig. 2. Reflected light OM microstructure of (a) BaO-excess, (b) TiO_2-excess single-layer samples sintered at 1365 °C/20 h in air, with higher magnifications shown in the inset. Respectively.

3.2. Embedded single-layer samples sintered at 1365 °C

When samples were sintered at 1365 °C/20 h, higher than the lowest eutectic of 1332 °C in the $BaTiO_3$–TiO_2 pseudo-binary system [14], the resultant microstructures of non-stoichiometric compositions (Fig. 2(a) for BaO-excess sample and Fig. 2(b) for TiO_2-excess sample) do not differ significantly. The fact that both samples are characterized by polygonal grains with rounded corners suggests a liquid-phase sintering mechanism. Monoclinic-Ba_2TiO_5 (B_2T) and monoclinic-$Ba_6Ti_{17}O_{40}$ (B_6T_{17}) second phases are detected by X-ray diffractometry (patterns not shown) in two single-layer samples. TiO_2-excess sample (Fig. 2(b)) has a larger average grain size of G_{av}=50 μm compared to G_{av}=39 μm of BaO-excess sample (Fig. 2(a)), although the latter of lower sintered density is apparent from the more extensive residual pores (Fig. 2(b)).

BaO-excess sample containing large grains with intra-granular residual pores suggests AGG (Fig. 2(a)). On the other hand, for TiO_2-excess sample it may be described as NGG (Fig. 2(b)) with residual pores still located at grain junctions, but in fact it consists of abnormal grains which have consumed the matrix grains and grown to larger sizes (~ 50 μm). Nevertheless, the grain size distribution of the two samples can be characterized by a normal distribution representing mono-modal in contrast to a bimodal in the solid-state sintered (Fig. 1(a)), or in liquid-assisted sintered (Fig. 1(b)) TiO_2-excess samples. An IGF of ~1.3 nm (Fig. 2(a)) and ~2.8 nm thickness (Fig. 2(b)), correspondingly, was found to exist along grain boundaries from samples of both compositions.

A superfluous quantity of intra-granular pores of very small size, i.e. < 5 nm, and irregular shape (not faceted [18]) is observed in both samples (foil #9 in Fig. 2(a) and #10 in Fig. 2(b)).

3.3. Two-layer samples embedded in BaO-excess powder sintered at 1365 °C

The cross-section microstructure of double-layer samples, embedded in BaO-excess powder and sintered at 1365 °C/1 h, is represented by Fig. 3; each layer at higher magnifications is shown in juxtaposition. Three regions across the sample thickness can immediately be discerned from the distinctive grain sizes. Surface region (region I) contains grains uniform in size (G_{av} = 40 μm) but smaller than those of region II; AGG is observed in both regions where intra-granular pores are discerned. Although region II contains grains grown to an average size G_{av} = 294 μm, region III shows extensive coarsening with the relative density remaining at $\rho_{rel} < 80\%$ whose microstructure is characterized by ubiquitous necking with NGG where intragranular pores are rarely observed. Similar to Fig. 2(b), it may also be that they are AGG grains (~20 μm) which have grown at the expense of smaller matrix grains. The microstructure resembles that observed in areas among the twin lamellae from samples of a similar composition but sintered at 1265 °C/20 h (Fig. 1(b)). Only region III not exhibiting the AGG characteristics may be described as NGG.

After prolonged sintering, the initially BaO-excess layer is similarly divided into two regions, region I and II (Fig. 4). The microstructure consists of polygonal grains after sintering was extended to 20 h. Regions made to FIB-foils are indicated in #'s corresponding to those in Table 1.

Grains in both region I and II contain intra-granular residual pores which is indicative of AGG, only that the average grain size differs significantly by G_{av} = 42 μm in region I and G_{av} = 263 μm in region II. Grains containing the {111} double-twin (as indicated) have a number frequency of ~53% in region I where those within an area of ~1 × 1 mm^2 were counted. Although residual pores entrapped in grain interior suggest that AGG has already begun, grains are still

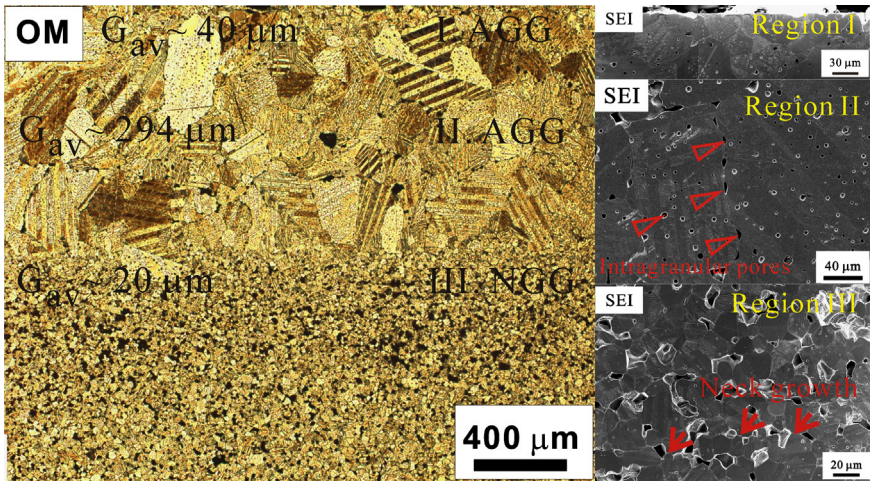

Fig. 3. Cross-section microstructure of two-layer sample sintered at 1365 °C/1 h. An overview reveals three regions of distinct grain sizes (reflected light OM), AGG in region I, and region II, and NGG and coarsened microstructure (SEM-SEI).

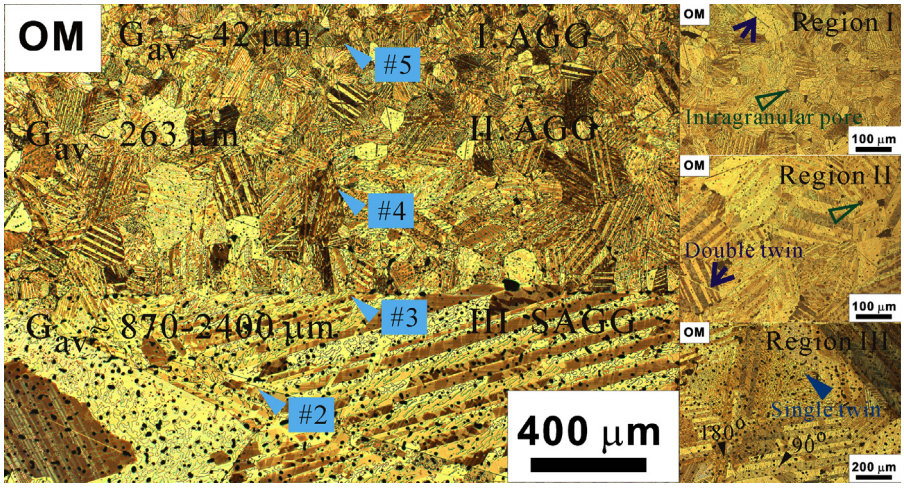

Fig. 4. Cross-section microstructure of two-layer sample embedded in BaO-excess powder and sintered at 1365 °C/20 h. An overview reveals three regions of distinct grain sizes with corresponding area at high magnifications showing AGG in region I, and region II, and SAGG in region III (reflected light OM).

Table 1
Thickness of IGF and FIB-foil positions of the corresponding sample.

Foil# Data	1	2	3	4	5	6	7	8	9	10	11	12
Sintering conditions	1215 °C/100 h	1365 °C/20 h				1365 °C/ 20 h	1365 °C/20 h		1365 °C/20 h	1365 °C/20 h	1265 °C/20 h	
Ba/Ti ratio	0.9889	1.0007				0.9889	0.9889		1.0007	0.9889	0.9889	
Interface and grain boundary with G_{av} (μm)	Bimodal	2400	AGG–SAGG	263	AGG–AGG	215	70	250	AGG–AGG of 40	NGG–NGG of 50	PAGG–NGG	TPRE
IGF (nm)	1.2	3.0	1.5	0.8	1.4	2.1	0.9	1.7	1.3	2.8	0.9	1.2
Boundary feature	Faceted	Faceted with glass pockets				Faceted	Faceted		Faceted with ledges		Faceted	
Sample type	Single-layer	Double layer				Single-layer	Double layer		Single-layer		Double layer	

rather uniform in size (Fig. 4) where the size distribution has not changed abruptly into a bimodal function.

Relative to those in region I, grains in region II have grown significantly. However, the number frequency of finding a {111} double-twinned grain at ~50% is almost the same. Ubiquitous residual pores are entrapped in grain interior, although some residual pores still remain located at triple grain junctions and along grain boundaries (as indicated in region II).

The microstructure of region III of the initially TiO_2-excess layer is represented very distinctly by extraordinarily large grains. They have grown to sizes between ~870 and 2400 μm (G_{av}=1330 μm) where intra-granular residual pores are profuse. The number frequency of finding a {111} double-twinned grain decreases to ~33%. Abnormally large grains containing intra-granular residual pores are the characteristic SAGG microstructure. Nevertheless, SAGG grains are not restricted to growing from double-twins, and single-twin boundaries [12] are indicated.

The Ba/Ti ratios determined using EDS from an average of five grains from regions I, II and III in Fig. 4 are 1.4164: 1.4322: 1.4162. Due to the overlapped EDS energy lines of Ba ($L\alpha$=4.465 keV) and Ti ($K\alpha$=4.508 keV), the results show considerable discrepancies with Ba/Ti=1.0007 and 0.9889 of the initial powders. However, they also suggest that the composition is being homogenized between layers upon sintering.

3.4. Two-layer samples embedded in TiO_2-excess powder sintered at 1365 °C

The sintered microstructure is divided into two layers with distinct grain sizes (Fig. 5), resembling Fig. 4, after sintering at 1365 °C/20 h. The BaO-excess layer-I reveals that double-twin grains do not necessarily lead to SAGG (as indicated), particularly when the re-entrant edges grow into ridges, as indicated. Further, not only are SAGG grains in the TiO_2-excess layer not as extensive as those shown in Fig. 4, but also large SAGG grains of e.g. ~1100 μm in size (layer-II in Fig. 5) remain surrounded by smaller grains (~70–100 μm). Besides, SAGG grains containing single-twin are often detected, as indicated.

3.5. Inter-granular glassy films

All grain boundaries examined under TEM contain a thin IGF. The thicknesses from eleven positions are ≤3.0 nm, as shown in Table 1. No dependence of G_{av} and thickness was found immediately.

Four grain boundaries (#2–#5) from two-layer sample shown in Fig. 4 were made to thin foils using FIB. Only one boundary (foil #3) is shown representatively for OF and UF images. Bright-field (BF) image of IGF at AGG–SAGG boundary (foil #3, Fig. 6) connecting a series of glass pockets shows that it is of ~1.5 nm thickness, shown in the inset. The high-resolution image of foil #3 shown in the inset (Fig. 6) confirms the IGF thickness determined by the Fresnel

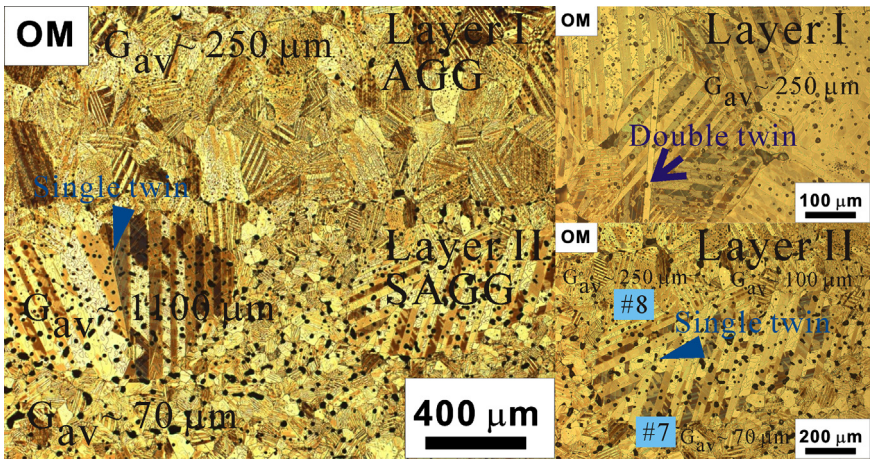

Fig. 5. Cross-section microstructure of two-layer sample embedded in TiO_2-excess powder and sintered at 1365 °C/20 h. An overview suggests two regions of distinctive grain sizes with corresponding area at high magnifications of AGG in region I and region II, and SAGG in region II (reflected light OM).

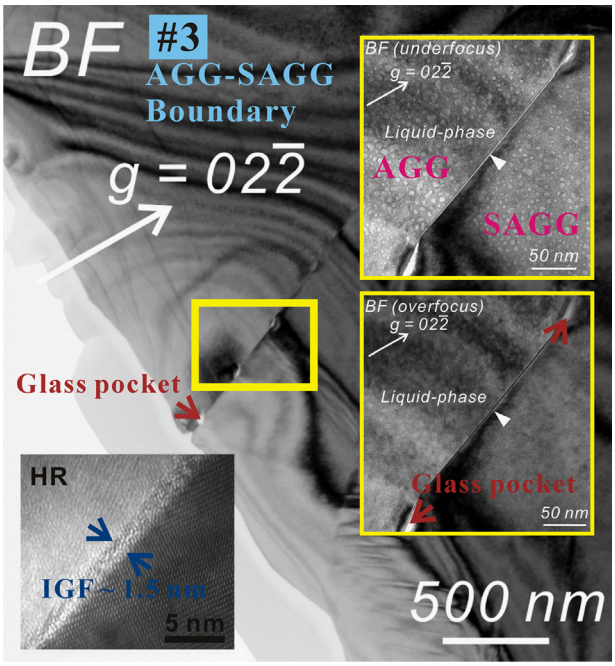

Fig. 6. IGF of ~1.5 nm thickness along AGG–SAGG interface (foil #3) (UF: under focus, OF: over focus, TEM-BF and high-resolution images). The locations of interfaces analyzed are indicated in Fig. 4.

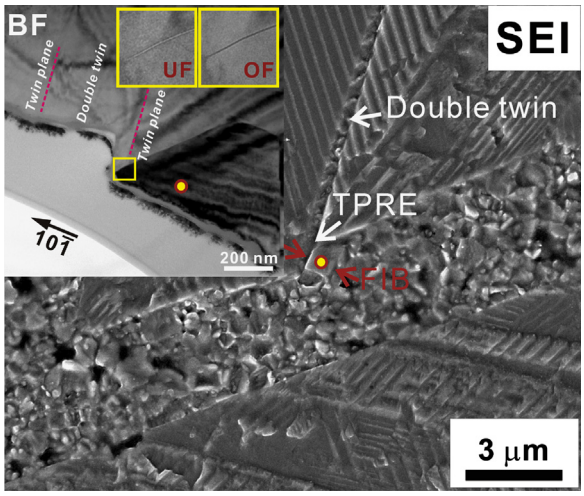

Fig. 7. Position of a TPRE edge shown indicated in SEM-SEI, and the presence of IGF at ~1.2 nm revealed by TEM-BF image (UF: under focus, OF: over focus).

technique [17]. And, IGF is ~3.0 nm thickness at boundary (foil #2) containing growth ledges between two SAGG grains. The wetting angle of $\phi = 0^\circ$ permits the eutectic liquid to penetrate into grain boundaries and spread over all grain surfaces.

Preparing FIB foils from TPRE edges was only successful after a few attempts. SEM indicating where the foil was made and TEM revealing the existence of IGF at the edges are shown in Fig. 7.

Numerous nano-scale intra-granular pores of < 5.0 nm size are again found in both grains across IGF in SAGG–SAGG and AGG–SAGG (Fig. 6) boundaries. This is strong evidence that residual pores were swept across by fast migrating boundaries containing liquids, a unique feature of AGG in ceramics. Growing $BaTiO_3$ single crystals via the SAGG route would suffer a major setback in crystal's quality [4].

4. Discussion

4.1. TPRE mechanism

Previous reports [1–3,9,10] suggested that perpetuated growth via TPRE during SAGG relies on the availability of the re-entrant corners provided by the {111} double-twin lamellae. It was claimed that when single-twin crystals grow into ridges, [9–11] they become less favorable for 2D nucleation, and consequently GG stops. The present observation does not entirely support this view because SAGG still occurs with single-twin grains [12], e.g., Fig. 5, because TiO_2-excess samples although containing {111} double-twins did not develop to SAGG even after annealing for 100 h (Fig. 1(a)) and 300 h [8] at 1215 °C (< 1260 °C). TPRE assumed [20]

that nucleation is rate-controlled for grains growing from melts, [19,20] or vapor phase [20]. While in Ostwald ripening, as happens here, either interface reaction (i.e. solution or reprecipitation) or diffusion in liquid phase may have been the rate-controlling step.

The number frequency of {111} double-twins grains is reduced from 53%, 50% of the AGG layer to 33% of the SAGG layer (Fig. 4). This may have indicated that the {111} twins grew among themselves facilitating SAGG. On the other hand, SAGG did not occur in single-layer samples regardless of the composition (Fig. 2(a) and (b)), neither in region I nor in region II of BaO-excess layer, even if they contained a sufficient quantity of double-twin grains (Fig. 4). Therefore, SAGG grains containing {111} single twins [12] (Fig. 5) suggest that 2D nucleation through TPRE is not the only mechanism responsible for SAGG in $BaTiO_3$. Examining TPRE edges from a double-twin lamellar grain corner, IGF (Fig. 7), serves as strong evidence that SAGG is encouraged by the presence of liquid phase.

4.2. Boundary mobility

The present results suggest that similar to Al_2O_3 [7,21], SAGG in $BaTiO_3$ is another convincing example of higher M_b magnified by a liquid grain boundary phase. Higher M_b facilitates faster GG rate and produces huge grains of ~2400 μm (2.4 mm) size (Fig. 4).

When a liquid film is present in polycrystalline ceramics, the boundary mobility (M_b) can be described [22] by

$$M_b = \frac{D_l C_l \Omega}{\omega k T} \quad (1)$$

where D_l is the diffusivity in liquid which is related to the viscosity (η) and particle radius (R) using the Stokes–Einstein equation $D_l = kT/6\pi R\eta$, C_l the solubility in liquid, Ω the atomic volume, ω the IGF thickness, and kT has its usual meaning.

The existence of IGF along the AGG–SAGG grain boundary (foil #3 in Fig. 6) is strongly supportive to the suggestion that the fastest moving boundaries in polycrystalline Al_2O_3 are impure and disordered [7,21]. According to Eq. (1), reducing IGF's thickness increases M_b direct-proportionally. However, IGF thicknesses detected from the interfaces ranging between ~0.9 and 3.0 nm (Table 1) do not differ significantly to completely justify the higher M_b (Eq. (1)) that leads to SAGG and extraordinarily large $BaTiO_3$ grains. Although IGF enhances M_b, it alone may not satisfactorily explain the SAGG in $BaTiO_3$. Even the glass viscosity (Eq. (1)) depending on the IGF composition may account for changes in M_b, and other causes must be sought.

4.3. Chemically induced grain growth via 2D faults

Anisotropic grain growth along directions parallel to the c-plane in ZnO ceramics is attributed [23] to the head-to-head inversion-domain boundaries (IDB) where the polar directions ($\pm$ c) have slower M_b than the non-polar directions. Similarly, the Ruddlesden–Popper (R–P) grains dispersed in the $SrTiO_3$ matrix are also characterized by a lamellar shape extending parallel to the (001) plane [24]. The R–P phase containing an interleaved rock-salt SrO-layer may be seen as the crystallographic shear (CS) structure.

When IGF and its effects on M_b cannot be ruled out in these ceramics, anisotropically grown grains also commonly contain planar faults. The {111} growth twins in $BaTiO_3$ [25] as a 2D growth fault containing a 2H (hexagonal in Ramsdell's notation) stacking sequence [25], and oxygen vacancies [26] may serve equivalently to facilitate AGG and PAGG (Fig. 1(a) and (b)), although not SAGG. The suggestion is that crystallographic faults such as IDB, growth twins, and the CS structure have non-stoichiometric compositions [24,25] or stacking faults [25,27] that provide favorable growth sites at low sintering temperatures, e.g., 1215 °C (Fig.1(a)) and 1265 °C (Fig. 1(b)) where eutectic liquids are not of significant amount to cover all grain boundaries. The AGG behavior may thus be termed as "chemically induced" planar growth. Nevertheless, grains [8] (Fig. 1(a)) did not coarsen into large sizes (Figs. 4 and 5) as in SAGG even after prolonged sintering for 100 h, and 300 h [8].

When sintering temperature is raised above 1265 °C (@1290 °C [28]), the characteristic {111} lamellar twin grains disappeared. That the {111} twin lamellae are altered into polygonal grains with the twinning retained is a common observation [28,29] in $BaTiO_3$ ceramics. It appears that the chemically induced growth mechanism is not conciliatory when the liquid phase is present. The AGG mechanism changes from that induced by growth faults (Fig. 1) to enhanced M_b by the liquid phase (Figs. 4 and 5) when liquid phase has a significant quantity, e.g., $T > 1265$ °C or with BaO-excess, that its effect on M_b becomes predominant. Examples of liquid-phase-enhanced growth in grains containing no crystallographic faults are indeed found in many other systems, e.g., $MgAl_2O_4$ spinel [30], Al_2O_3 [31], and Si_3N_4 [32].

5. Conclusions

AGG including PAGG and SAGG in $BaTiO_3$ ceramics is examined in sintered $BaTiO_3$ ceramics via microscopic observation using OM, SEM and TEM.

TPRE may not be the only mechanism that leads to SAGG in $BaTiO_3$ ceramics. Similar to converting polycrystalline Al_2O_3 into single-crystal sapphire, SAGG in $BaTiO_3$ through Ostwald ripening necessitates faster boundary mobility via IGF. The IGF between ~0.9 and 3.0 nm thickness significantly increases M_b. However, it alone cannot fully account for the grain growth rate that produces extraordinarily large grains. Although a synergistic effect combining narrow IGF with lower viscosity eutectic liquids, higher diffusivity and higher solubility in the liquid may all contribute to the mobility enhancement that facilitates SAGG, further studies are necessary.

An AGG mechanism involving chemically induced growth faults, i.e., the {111} growth twins, may also have a role in instigating PAGG, particularly at low-temperature sintering

when the liquid phase exists in small quantities. At higher sintering temperatures, e.g., $T > 1265$ °C, liquid-phase-enhanced M_b contributes more significantly to SAGG in $BaTiO_3$ ceramics. A sufficient quantity of BaO is necessary for the ternary eutectic reaction with trace impurity SiO_2 to catalyze SAGG. This additional BaO is supplied by embedding TiO_2-excess $BaTiO_3$ samples in BaO-excess powder during sintering.

Acknowledgments

A research funding provided by the National Science Council of Taiwan through NSC-100-2221-E-110-051-MY3 is acknowledged.

References

[1] Y.S. Yoo, H. Kim, D.Y. Kim, Effect of SiO_2 and TiO_2 addition on the exaggerated grain growth of $BaTiO_3$, Journal of the European Ceramic Society 17 (6) (1997) 805–811.
[2] M.K. Kang, Y.S. Yoo, D.Y. Kim, N.M. Hwang, Growth of $BaTiO_3$ seed grains by the twin-plane re-entrant edge mechanism, Journal of the American Ceramic Society 83 (2) (2000) 385–390.
[3] H.Y. Lee, J.S. Kim, D.Y. Kim, Effect of twin-plane re-entrant edge on the coarsening behavior of barium titanate grains, Journal of the American Ceramic Society 85 (4) (2002) 977–980.
[4] T. Yamamoto, T. Sakuma, Fabrication of $BaTiO_3$ single crystal by solid-state grain growth, Journal of the American Ceramic Society 77 (4) (1994) 1107–1109.
[5] C. Scott, M. Kaliszewski, C. Greskovich, L. Levinson, Conversion of polycrystalline Al_2O_3 to single crystal sapphire by abnormal grain growth, Journal of the American Ceramic Society 85 (5) (2002) 1275–1280.
[6] C. Greskovich, J. Brewer, Grain boundary migration at high speed in Al_2O_3, Journal of the American Ceramic Society 90 (5) (2007) 1375–1381.
[7] S.J. Dillon, M.P. Harmer, Mechanism of solid-state single-crystal conversion in alumina, Journal of the American Ceramic Society 90 (3) (2007) 993–995.
[8] M.H. Lin, J.F. Chou, H.Y. Lu, Grain growth inhibition in Na_2O-doped TiO_2-excess $BaTiO_3$ ceramic, Journal of the American Ceramic Society 83 (9) (2000) 2155–2162.
[9] D.R. Hamilton, R.G. Seidensticker, Propagation mechanism of germanium dendrite, Journal of Applied Physics 31 (7) (1960) 1165–1168.
[10] R. Jagannathan, R.V. Mehta, J.A. Timmons, D.L. Black, Anisotropic growth of twinned cubic crystals, Physical Review B 48 (18) (1993) 13261–13265.
[11] K. Fujiwara, K. Maeda, N. Usami, K. Nakajima, Growth mechanism of Si-faceted dendrites, Physical Review Letters 101 (5) (2008) 055503-1–055503-4.
[12] J. Munoz-Saldana, B. Mullier, G.A. Schneider, Preparation of $BaTiO_3$ single crystals using the modified SiO_2 exaggerated grain growth method, Journal of the European Ceramic Society 22 (5) (2002) 681–688.
[13] D.E. Rase, R. Roy, Phase equilibrium in the system $BaTiO_3$–SiO_2, Journal of the American Ceramic Society 38 (11) (1955) 389–395.
[14] K.W. Kirby, B.A. Wechsler, Phase relations in $BaTiO_3$–TiO_2 system, Journal of the American Ceramic Society 74 (8) (1991) 1841–1847.
[15] C. Greskovich, K.W. Lay, Grain growth in very porous Al_2O_3 compacts, Journal of the American Ceramic Society 55 (3) (1972) 142–146.
[16] S.Y. Cheng, N.J. Ho, H.Y. Lu, Transformation induced twinning: The 90° and 180° ferroelectric domains in $BaTiO_3$, Journal of the American Ceramic Society 89 (7) (2006) 2177–2187.
[17] D.R. Clarke, Observation of microcracks and thin intergranular films in ceramics by TEM, Journal of the American Ceramic Society 63 (1–2) (1980) 104–106.
[18] H.W. Lee, M.S.H. Chu, H.Y. Lu, Intragranular voids and dc degradation in (CaO+MgO) codoped $BaTiO_3$ multilayer ceramic capacitors, Journal of the American Ceramic Society 92 (12) (2009) 3037–3043.
[19] J.M. Howe, Interfaces in Materials, J. Wiley, New York71–149.
[20] D.A. Porter, K.E. Easterling, Phase Transformation in Metals and Alloys, Chapman and Hall, London, England199–203.
[21] S.J. Dillon, M.P. Harmer, Intrinsic grain boundary mobility in alumina, Journal of the American Ceramic Society 89 (12) (2006) 3885–3887.
[22] M. Yan, R.M. Cannon, H.K. Bowen, Grain boundary migration in ceramics, in: R.M. Fulrath, J.A. Pask (Eds.), Ceramic Microstructure '76, Westview, Boulder, CO, 1977, pp. 276–307.
[23] J.S. Lee, S.M. Wiederhorn, Effects of polarity on grain-boundary migration in ZnO, Journal of the American Ceramic Society 87 (7) (2004) 1319–1323.
[24] C.H. Nien, H.Y. Lu, Crystallographic orientation relationships between $SrTiO_3$ and ruddlesden-popper phase, Journal of the American Ceramic Society 95 (5) (2012) 1676–1681.
[25] Y.C. Wu, C.C. Lee, H.Y. Lu, D.E. McCauley, M.S.H. Chu, The {111} growth twins in tetragonal $BaTiO_3$, Journal of the American Ceramic Society 89 (5) (2006) 1679–1686.
[26] C.L. Jia, K. Urban, Atomic-resolution measurement of oxygen concentration in oxide materials, Science 303 (5666) (2004) 2001–2004.
[27] A. Recnik, D. Kolar, Exaggerated grain growth in hexagonal $BaTiO_3$ under reducing sintering conditions, Journal of the American Ceramic Society 79 (4) (1996) 1015–1018.
[28] J.K. Liou, M.H. Lin, H.Y. Lu, Crystallographic facetting in sintered $BaTiO_3$, Journal of the American Ceramic Society 85 (12) (2002) 2931–2937.
[29] L.A. Xue, in: Additives and the Control of Grain Growth in $BaTiO_3$, University of Leeds, U.K., 1987 Ph.D. thesis.
[30] Y.M. Chiang, W.D. Kingery, Grain boundary migration in nonstiochiometric solid solution of magnesium aluminate spinel: I, grain growth studies, Journal of the American Ceramic Society 72 (2) (1989) 271–277.
[31] H. Song, R.L. Coble, Origin and growth of plate-like abnormal grains in liquid-phase-sintered alumina, Journal of the American Ceramic Society 73 (7) (1990) 2077–2085.
[32] H.-J. Kleebe, Comparison between SEM and TEM imaging techniques to determine grain-boundary wetting in ceramic polycrystals, Journal of the American Ceramic Society 85 (1) (2002) 43–48.